Heterogeneous InGaAs/SiC UTC-PDs with Array Antennas Enabling On-Chip THz Wireless Communication

Che, Ming
Graduate School of Information Science and Electrical Engineering, Kyushu University

Kamiura, Yoshiki
Graduate School of Information Science and Electrical Engineering, Kyushu University

Li, Yuanhao
Graduate School of Information Science and Electrical Engineering, Kyushu University

Kato, Kazutoshi
Graduate School of Information Science and Electrical Engineering, Kyushu University

https://hdl.handle.net/2324/7402140

出版情報：pp.306-309, 2025-11-19. IEEE
バージョン：
権利関係：

Heterogeneous InGaAs/SiC UTC-PDs with Array Antennas Enabling On-Chip THz Wireless Communication

Ming Che#, Yoshiki Kamiura, Yuanhao Li, Kazutoshi Kato
Graduate School of Information Science and Electrical Engineering,
Kyushu University, Japan
#che.ming.677@m.kyushu-u.ac.jp

***Abstract*— This study presents a compact on-chip THz source achieved by monolithically integrating InGaAs/SiC UTC-PDs with a planar antenna array. The high thermal conductivity of the SiC substrate enhances the saturation photocurrent, enabling stable high-power operation. A microstrip Y-branch structure combines the output power of two UTC-PDs with minimal insertion loss, while the planar antenna array improves beam directivity. The device achieves a 3 dB bandwidth of 25 GHz centred around 290 GHz, with a half-power beamwidth of 60° and an 8 dB side-lobe level. Wireless communication experiments at 290 GHz demonstrate bit error rates below the 7% HD-FEC thresholds at data rates of 10 Gbit/s. These results highlight the device's potential for next-generation high-speed wireless communication systems.**

***Keywords*— THz, Array Antenna, UTC-PD, SiC, Combining.**

I. Introduction

THz waves, located between microwaves and infrared radiation in the electromagnetic spectrum, offer a unique combination of wide bandwidth and high spatial resolution, making them highly suitable for ultra-high-speed wireless communication, non-invasive imaging, and advanced sensing applications. Among various THz generation techniques, uni-traveling-carrier photodiodes (UTC-PDs) [1], [2] stand out due to their ability to produce tunable and coherent THz signals by mixing two lasers with slightly different frequencies. However, the inherently low output power of these sources, combined with the significant absorption of THz waves by atmospheric water vapor, presents a critical challenge for long-range communication and high-sensitivity detection. To overcome this limitation, it is essential to improve both the generation efficiency and radiation performance of THz sources.

Achieving efficient, low-loss radiation is challenging because the antenna structure's dimensions are comparable to or smaller than the THz wavelength. However, this size characteristic enables the monolithic integration of nanoscale InGaAs/SiC UTC-PDs with planar antennas. Such chip-level integration [3], [4], [5] shortens the electromagnetic transmission path, reducing energy loss from impedance mismatches and improving coupling efficiency, thereby enhancing energy efficiency and bandwidth. Typically, UTC-PDs are integrated with waveguide [6], [7] or lens [8], [9] outputs. Waveguides offer high transmission efficiency and low radiation loss for long-distance transmission, while lenses provide wider radiation angles and uniform field distribution for large-area coverage. However, both are physically larger than the THz wavelength, limiting miniaturization and seamless integration with other electronic and photonic components. Therefore, developing compact, high-performance on-chip THz sources [10], [11] is essential for overcoming these limitations and advancing next-generation wireless communication devices.

This study aims to develop a compact and efficient on-chip THz source by monolithically integrating UTC-PDs with a planar array antenna, as conceptually illustrated in Fig. 1. First, the high thermal conductivity of the SiC substrate enhances the saturation photocurrent of each UTC-PD, enabling stable high-power operation. Second, the transmission-line power-combining network integrates the output power of multiple UTC-PDs, effectively increasing the overall output while minimizing insertion loss. Third, the planar antenna array improves the directivity of the radiated THz beam, enhancing the relative output power and ensuring efficient free-space propagation. This integrated design is expected to drive the next generation of wireless communication devices

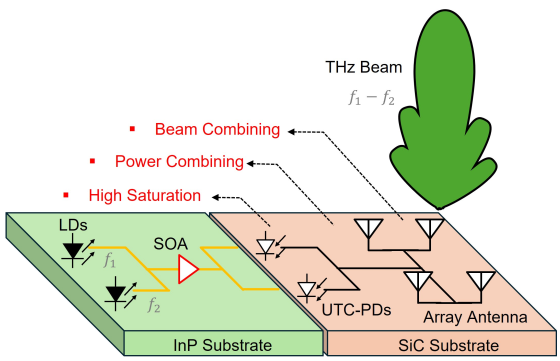

Fig. 1. Conceptual diagram of the heterogeneous integration of UTC-PDs with an array antenna for on-chip THz wireless transmission, achieved through enhanced saturation output power of individual UTC-PDs, power combining via transmission lines, and beam combining by the antenna array. (LDs: Laser Diodes, SOA: Semiconductor Optical Amplifier, UTC-PD: uni-traveling-carrier photodiode.)

toward higher data rates, compact form factors, and improved energy efficiency.

II. Design and Fabrication

Figs. 2(a) and (b) present the top and cross-sectional views of the proposed design, featuring two InGaAs/SiC UTC-PDs integrated with a 2×2 microstrip patch antenna (MPA) array on a silicon carbide (SiC) substrate. The UTC-PDs and MPA array are fabricated on a 32 μm thick SiC layer, forming a sandwich configuration that enhances the performance of individual UTC-PDs by improving heat dissipation and reducing energy loss. The high thermal conductivity of SiC enables efficient heat removal, which increases the saturation photocurrent and subsequently enhances the output power of each UTC-PD. Additionally, the direct on-chip integration of UTC-PDs with the antenna array minimizes transmission loss compared to conventional wire bonding techniques, which are often associated with higher insertion loss and impedance mismatch. This structural design is crucial for sustaining the increased power output achieved by combining the outputs of two UTC-PDs through a microstrip Y-branch structure, which serves as a power-combining network with minimal insertion loss during signal synthesis. The antenna array is precisely engineered to maximize gain in the broadside direction, with the spacing between the four inset-patch MPAs, optimized to reduce mutual coupling while maintaining constructive interference. Each inset patch is strategically recessed from one edge toward the center, ensuring a precisely matched feed path for the MSL, thereby enhancing impedance matching and radiation efficiency.

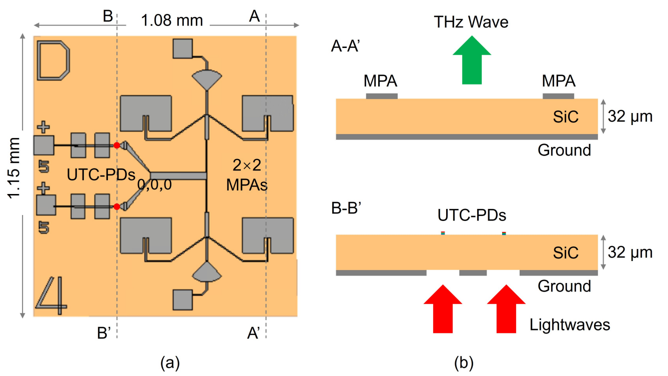

Fig. 2. Top and cross-sectional views of the designed chip-scale THz source, where two InGaAs UTC-PDs are integrated with a 2x2 MPA array on an SiC substrate.

The exceptional thermal conductivity of 4H-SiC, approximately 490 W/(m·K) at room temperature, ensures efficient heat dissipation in high-power THz devices, thereby maintaining device stability and performance. However, its high Mohs hardness of 9.5 presents significant challenges for conventional fabrication techniques, as precise micromachining of fine structures is difficult to achieve. To overcome this challenge, advanced wafer bonding techniques are employed to integrate InGaAs UTC-PD epitaxial layers onto the SiC substrate. As shown in Fig. 3, the flip-wafer bonding process begins with the epitaxial growth of InGaAs UTC-PD layers on an InP substrate, which serves as a temporary growth platform. A thin SiO_2 layer is deposited on top of the epitaxial layers to provide mechanical support and promote adhesion during the transfer process. The entire structure is then inverted and bonded onto the SiC substrate under high pressure and elevated temperature, ensuring atomic-level adhesion at the interface. After bonding, the InP substrate is selectively removed through chemical etching, leaving the UTC-PD epitaxial layers seamlessly transferred onto the SiC substrate while the SiO_2 layer is retained as a buffer layer to mitigate thermal stress and lattice mismatch.

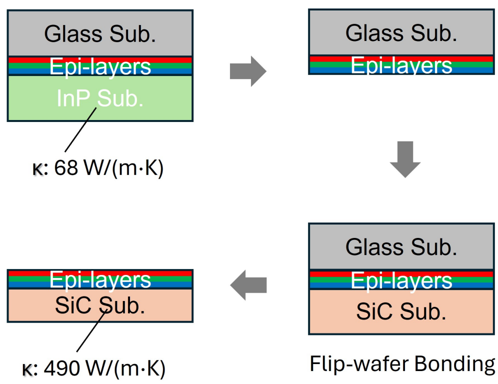

Fig. 3. Illustration of the substrate-transfer technique using flip-wafer bonding to integrate InGaAs UTC-PD layers onto the SiC substrate.

III. Experimental Setup

The experimental setup, illustrated in Fig. 4, is designed to evaluate the characteristics and on-chip wireless communication capabilities of the fabricated chip, focusing on the generation, transmission, and detection of THz signals. Two tunable wavelength laser diodes (LDs) generate an optical

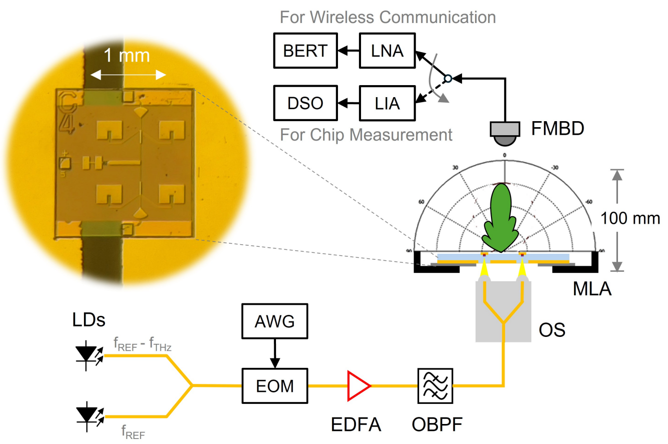

Fig. 4. Experimental setup for the characterization and on-chip wireless communication of the developed THz source, including a microscopic view of the fabricated chip. (AWG: arbitrary waveform generator, EOM: electro-optical modulator, EDFA: erbium-doped fiber amplifier, OBPF: optical bandpass filter, OS: optical splitter, FMBD: Fermi-level managed barrier diode, LIA: lock-in amplifier, DSO: digital storage oscilloscope.)

beat signal at the desired THz frequency f_{THz}. One LD is tuned to a reference frequency f_{ref} of 193.4 THz, while the other is set to $f_{\mathrm{ref}} - f_{\mathrm{THz}}$. For chip measurements, an arbitrary waveform generator (AWG) modulates the optical signal at 1 MHz using an electro-optic modulator (EOM) to reduce environmental noise during lock-in detection. The modulated signal is then amplified by an erbium-doped fiber amplifier (EDFA) to increase its intensity, and an optical bandpass filter (OBPF) suppresses spontaneous emission noise, ensuring a low phase noise optical beat signal. The amplified optical signal is subsequently divided into four equal parts using a 1×4 optical splitter, with each output port of the splitter attached to a collimation lens. Each lens is spaced at 250 µm intervals, ensuring precise alignment with the chip's photodiode regions. The emitted THz radiation is detected using a Fermi-level managed barrier diode (FMBD), which converts the THz power into an electrical signal. Finally, a lock-in amplifier (LIA) processes the electrical signal, significantly enhancing the signal-to-noise ratio and enabling accurate measurements of the THz radiation performance. For wireless communication experiments in the THz frequency range, the AWG is used to generate on-off keying (OOK) modulation signals at data rates in the Gbit/s range. This setup allows the evaluation of the chip's ability to transmit and receive high-speed wireless data while maintaining low bit error rates, demonstrating its potential for next-generation THz communication systems.

IV. Measurements and Wireless Application

Fig. 5 illustrates the measured frequency dependence of the generated power gain across the range of 260–320 GHz, highlighting the key operational characteristics of the THz chip. During the measurement, the UTC-PD chip was biased at -1 V, with a photocurrent of 5 mA. The 3 dB bandwidth, centered around 290 GHz, is approximately 25 GHz. Beyond 310 GHz, the power gain drops sharply, which may result from the combined effects of the antenna's resonance frequency shift and the frequency dependence of the UTC-PD output, where the gain decreases as the coupling signal bandwidth increases.

Fig. 6 illustrates the relationship between THz power gain and photocurrent for the UTC-PD under different bias voltages ranging from 0.6 V to 1.2 V. The THz gain increases with photocurrent across all bias conditions, reaching saturation at approximately 10 mA. At lower photocurrents ranging from 0 to 2 mA, the gain rises rapidly. As the photocurrent increases beyond 6 mA, the gain gradually approaches a plateau, suggesting that the UTC-PD's carrier transport and thermal dissipation capabilities limit further gain improvement. Among the tested bias voltages, -1.2 V yields the highest saturation gain, demonstrating that a stronger electric field enhances carrier acceleration and THz emission.

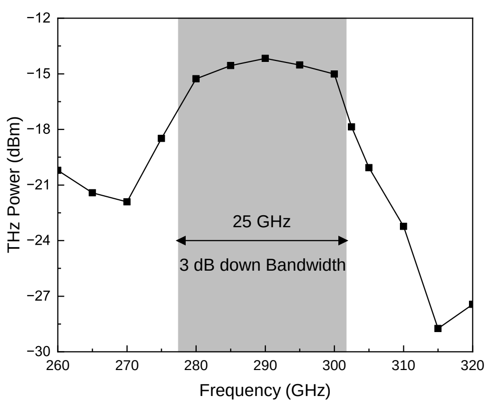

Fig. 5. Measured frequency dependance of the generated power gain across the 260–320 GHz range.

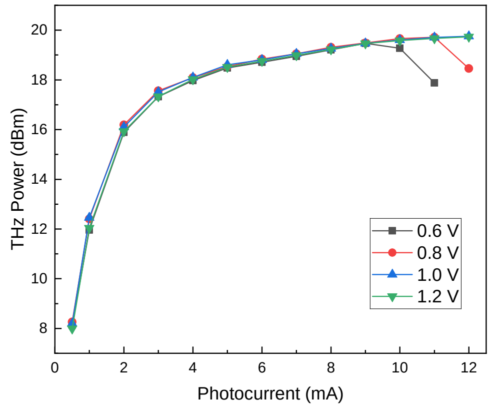

Fig. 6. Measured THz output power versus photocurrent under different bias voltages ranging from 0.6 V to 1.2 V.

Fig. 7 illustrates the measured E- and H-field radiation patterns of the 2×2 MPA array at 290 GHz. The E-plane pattern, shown in black, and the H-plane pattern, shown in red, both exhibit directional radiation with main lobes centered around the broadside direction (0°). The 3 dB beamwidth is approximately 60° for both planes, indicating good directivity suitable for directional THz wireless transmission. The side-lobe level (SLL) is approximately 8 dB, representing the difference between the main lobe's peak gain and the highest sidelobe, which ensures relatively low interference from sidelobes.

Fig. 8 illustrates the measured bit error rate (BER) as a

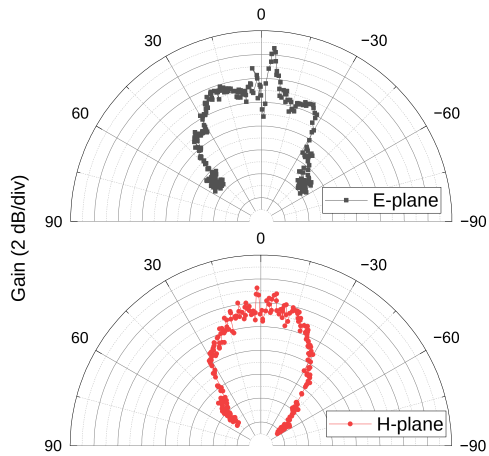

Fig. 7. Measured E- and H-field radiation patterns at 290 GHz.

function of transmission rate at different photocurrents for a 290 GHz carrier over a 300 mm transmission distance. The BER decreases as the transmission rate increases up to a certain point, after which it rises due to increased data throughput and corresponding signal degradation. At a photocurrent of 3.7 mA, the system achieves the lowest BER across the entire transmission range, maintaining a BER below the 7% HD-FEC threshold up to approximately 10 Gbit/s and below the 20% SD-FEC threshold up to about 11 Gbit/s. The inset shows an eye diagram measured at a photocurrent of 3.7 mA and a transmission rate of 10 Gbit/s, with an eye amplitude of 291 mV and a signal-to-noise ratio (SNR) of 10.5 dB. The well-defined eye opening demonstrates clear signal integrity, supporting the low BER observed at this operating condition. However, at 1.7 mA, the BER remains above both FEC thresholds across most of the measured range, indicating insufficient power for reliable high-speed transmission. These results highlight the system's capability to achieve high-speed wireless communication at 290 GHz, with increased photocurrent enabling higher transmission rates while maintaining acceptable BER levels within standard FEC thresholds.

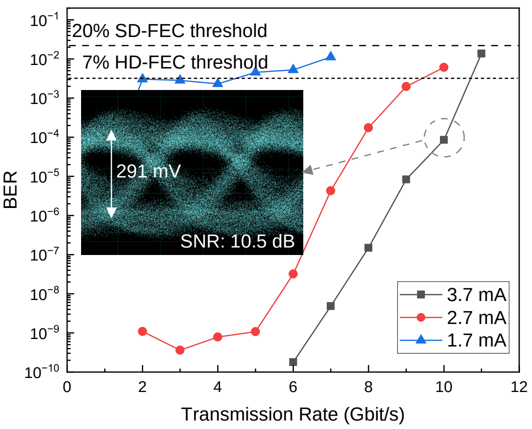

Fig. 8. Measured bit error rate (BER) versus transmission rate at different photocurrents for a 290 GHz carrier over a 300 mm transmission distance, with 7% HD-FEC and 20% SD-FEC thresholds indicated. The inset shows an eye diagram measured at 3.7 mA and 10 Gbit/s.

V. Conclusion

This study successfully demonstrates a compact on-chip THz source by monolithically integrating InGaAs/SiC UTC-PDs with a planar antenna array. The high thermal conductivity of the SiC substrate enhances the saturation photocurrent, enabling stable high-power operation, while the transmission-line power-combining network effectively increases the output power with minimal insertion loss. The planar antenna array improves the directivity of the radiated THz beam, achieving a 3 dB beamwidth of approximately 60° and an 8 dB side-lobe level, supporting efficient free-space propagation. The device exhibits a 3 dB bandwidth of about 25 GHz centered around 290 GHz, with a maximum output power obtained at a bias voltage of -1.2 V and a photocurrent of 10 mA. Wireless communication experiments demonstrate reliable data transmission at 290 GHz, achieving BERs below the 7% HD-FEC and 20% SD-FEC thresholds at data rates of 10 Gbit/s and 11 Gbit/s, respectively. These results validate the potential of the developed THz source for next-generation wireless communication systems, offering high data rates, compact integration, and enhanced energy efficiency, paving the way for advanced applications in high-speed wireless networks and beyond.

Acknowledgment

This work was supported by the National Institute of Information and Communications Technology (NICT) under commissioned research projects JPJ012368C00901 and JPJ012368C02801, as well as by MIC/SCOPE Grant #195010002 and JSPS KAKENHI Grants 23K17751 and 24K17324. The authors would like to express their sincere gratitude to Prof. T. Nagatsuma of The University of Tokyo and Dr. T. Ishibashi of Wavepackets LLC for their contributions to the development of the UTC-PD, and to Prof. H. Ito of The University of Tokyo for providing the FMBD.

References

[1] T. Nagatsuma, G. Ducournau, and C. C. Renaud, "Advances in terahertz communications accelerated by photonics," Nature Photonics, vol. 10, no. 6, pp. 371–379, 2016.

[2] T. Ishibashi and H. Ito, "Uni-traveling carrier photodiodes: Development and prospects," IEEE Journal of Selected Topics in Quantum Electronics, vol. 28, no. 2: Optical Detectors, pp. 1–6, 2021.

[3] C. C. Renaud et al., "Antenna integrated THz uni-traveling carrier photodiodes," IEEE Journal of Selected Topics in Quantum Electronics, vol. 24, no. 2, pp. 1–11, 2017.

[4] M. Che, K. Kondo, and K. Kato, "Generating and Enhancing THz Pulses via an Antenna-Coupled Unitraveling-Carrier Photodiode Array," IEEE Transactions on Terahertz Science and Technology, vol. 13, no. 3, pp. 280–285, 2023.

[5] M. Che, K. Kondo, R. Doi, and K. Kato, "Demonstration of Optoelectronic-Phased-Array Driven THz-wave Power Combination and Beam Steering," in Optical Fiber Communication Conference, Optica Publishing Group, 2023, pp. M3D-4.

[6] H. Ito et al., "Photonic millimetre-and sub-millimetre-wave generation using J-band rectangular-waveguide-output uni-travelling-carrier photodiode module," Electronics Letters, vol. 42, no. 24, pp. 1424–1425, 2006.

[7] T. Nagatsuma et al., "600-GHz-band waveguide-output uni-traveling-carrier photodiodes and their applications to wireless communication," in 2018 IEEE/MTT-S International Microwave Symposium-IMS, IEEE, 2018, pp. 1180–1183.

[8] H. Ito, T. Yoshimatsu, and T. Ishibashi, "Broadband photonic terahertz-wave emitter based on planar-antenna-integrated UTC-PD," in Terahertz Emitters, Receivers, and Applications IV, 2013, pp. 54–63.

[9] K. Konstantinidis et al., "Low-THz dielectric lens antenna with integrated waveguide feed," IEEE transactions on Terahertz Science and Technology, vol. 7, no. 5, pp. 572–581, 2017.

[10] M. Che et al., "450-GHz-wave beam-steering with 1 kHz repetition by optical phase control," in 45th European Conference on Optical Communication (ECOC 2019), IET, 2019, pp. 1–3.

[11] M. Che, H. Kanaya, and K. Kato, "Optically controlled THz power tuning based on interference at transmission line," Optics Express, vol. 29, no. 13, pp. 20034–20044, 2021.